Polymer Testing 95 (2021) 107136

Contents lists available at ScienceDirect

Polymer Testing

journal homepage: http://www.elsevier.com/locate/polytest

Toughening of polylactide by *in-situ* reactive compatibilization with an isosorbide-containing copolyester

Chang Kyu Park [a], Dong Jin Jang [a,b], Joo Hyung Lee [a], Seong Hun Kim [a,b,*]

[a] Department of Organic and Nano Engineering, Hanyang University, Seoul, 04763, Republic of Korea
[b] Human-Tech Convergence Program, Hanyang University, Seoul, 04763, Republic of Korea

ARTICLE INFO

Keywords:
Polylactide (PLA)
Poly(1,4-cyclohexanedimethylene isosorbide terephthalate) (PEICT)
Polymer blends
In-situ compatibilization
Impact strength

ABSTRACT

Polylactide (PLA)/poly(1,4-cyclohexanedimethylene isosorbide terephthalate) (PEICT) blends were prepared by melt processing. Oligomer, with multiple epoxy functional groups, were introduced as a reactive compatibilizer to enhance interfacial adhesion of the two blend components. The reaction between the reactive compatibilizer and blend components was confirmed by infrared spectroscopy and rheological analysis. The improved compatibility of the blends reduced interfacial tension between polymer components, yielding a co-continuous phase morphology from a sea–island morphology. The added PEICT improved the impact strength of PLA to 22.5 kJ/m^2 at 40% loading. After compatibilization and the impact strength of PLA/PEICT blends increased to 44.1 kJ/m^2, showing that increased interfacial adhesion improved energy transfer between the polymers.

1. Introduction

Commodity polymers with its light weight and good mechanical properties are crucial components of many industries, including agriculture, packaging, medicine, electronics, and automobiles [1]. However, these petroleum-derived materials cause environmental pollution because of their large carbon footprints and accumulation of post-consumer waste [2,3]. Such apprehensions have stimulated numerous regulations on petroleum-based materials, and the use of sustainable biobased materials is being encouraged. Polylactide (PLA; presented in Scheme 1) is a sustainable polyester synthesized from biomass-derived lactic acid and is a promising replacement for petroleum-based commodity polymers. PLA is a linear aliphatic polyester with excellent mechanical properties and biocompatibility; however, its inherent brittleness, poor thermal stability, and low crystallization rate restrict its widespread use [4–6]. To overcome these obstacles to commercial use, modifications such as copolymerization [7–9], blending [9–11], plasticization [12–16], and the incorporation of reinforcements have been made [2–4,17–21].

The plasticization of polymers is commonly used to aid processing and improve ductility and flexibility to their final performance. However, plasticizers typically have comparably low molecular weights than polymers and are prone to migration into other media, resulting in performance loss over time [22,23]. The incorporation of nanofillers such as carbon nanotubes (CNT) can increase the crystallization rate and overall mechanical properties, but issues such as aggregation remain an obstacle to industrialization [3,24]. However, the blending of PLA with ductile and flexible polymers is a cost-effective and straightforward method to modify the properties. Polymers such as polycaprolactone (PCL) [25–27], poly(butylene succinate) (PBS) [28,29], poly(ethylene terephthalate) [29], thermoplastic starch [31], polyamide 11 (PA11) [32], and poly(butylene adipate-*co*-terephthalate) (PBAT) [33,34] have been investigated as components for blending with PLA.

Recently, SK Chemical Co., Ltd successfully commercialized the amorphous copolyester poly(1,4-cyclohexanedimethylene isosorbide terephthalate) (PEICT; presented in Scheme 1) under the trade name ECOZEN® [35]. Isosorbide is a biobased diol with a bicyclic ring structure of two tetrahydrofuran units. When incorporated in the backbone of the polymer, the rigid structure and chirality of isosorbide can enhance the glass transition temperature (T_g) and transparency. 1, 4-Cyclohexane dimethanol is known for its two conformations, the e, e-trans cyclohexylene structure and a,a-*trans*-cyclohexylene ring twisted-boat form [36–38]. Such conformational transitions result in significant chain mobility to the cyclic structure, enhancing the relaxation and giving the final polymer a high impact strength with high melting temperature. Such attributes give PEICT high heat resistivity, high transparency, and excellent impact properties. These characteristics make PEICT an excellent candidate for blending with PLA, however

* Corresponding author.
E-mail address: kimsh@hanyang.ac.kr (S.H. Kim).

https://doi.org/10.1016/j.polymertesting.2021.107136
Received 1 December 2020; Received in revised form 4 February 2021; Accepted 18 February 2021
Available online 23 February 2021

to the author's knowledge such attempt has not yet been reported.

Although polymer blending can effectively enhance the mechanical properties, the poor compatibility of the blend components can lead to unsatisfactory mechanical properties. The structural difference between the two blend components is the main cause of the poor compatibility, resulting in the aggregation of the minor component in the main polymer matrix [39]. Therefore, improving the interfacial adhesion of the polymer blends has been the focus of polymer blending research. Traditionally, immiscible blends have been compatibilized using block or graft copolymers made of polymers with high interfacial affinity for each blend component. However, the use of copolymer compatibilizers requires an additional step of synthesizing the copolymer compatibilizer, thus increasing the time and cost of production. The addition of a crosslinking agent or chain extender to the blending process can reduce this synthesis process and effectively improve the interfacial adhesion in the immiscible polymer blends.

Various *in-situ* reactive agents have been explored for the compatibilization of PLA blends. The free-radical initiator dicumyl peroxide has been repeatedly investigated for its use as reactive compatibilization of PLA with rubbery polymers [20,28,40,41]. However, free radical initiators with low decomposition temperature can decompose prematurely, resulting in inefficient compatibilization [20,28,42,43]. Reactive compatibilization with multifunctional isocyanates can effectively enhance the miscibility of PLA blends with -OH terminated polymers [25,26,44]. Nonetheless, the high toxicity and volatility of isocyanates can cause serious health issues, limiting their use in polymer blends. Recently, a group of chain extending and crosslinking agents containing epoxy groups under the trade name JONCRYL ADR® (ADR; presented in Scheme 1) have drawn extensive interest for the compatibilization of PLA. Baimark et al. prepared blends of the two stereoisomeric PLA, and Lin et al. prepared PLA blended with polycarbonate (PC) to improve the thermal properties of PLA using styrene-acrylic multifunctional oligomeric agent [45]. Walha et al. reported on the formation of copolymers by ADR at the interface of the PLA/PA11 blends, which reduced the size and interfacial tension [46]. Yu et al. prepared high-performance ADR compatibilized PLA/PA11 blends with impact strength values of 77.57 MPa [32]. Li et al. and Wang et al. reported the effect of ADR on the blends of PLA/PBAT and discussed the toughening mechanism of the blends [39,47,48].

In this work, blends of PLA and PEICT with varying ratios were prepared and investigated for their mechanical and thermal properties. ADR was used as an *in-situ* compatibilizer (Scheme 2 [49]) to enhance the interfacial affinity of the PLA/PEICT blends. The surface energy of the blend components was investigated to understand the compatibilization reaction, and Fourier transform infrared (FTIR) spectroscopy and rheological analysis were used to confirm the presence of the reaction. The PLA/PEICT blends exhibited greatly enhanced impact properties after compatibilization.

2. Experimental

2.1. Materials and preparations

PLA (2003D; specific gravity = 1.24 g/cc, melt flow index (MFI) at 210 °C = 6 g/10 min) and PEICT (Ecozen T90; specific gravity = 1.25 g/cc, MFI at 230 °C = 10.9 g/10 min) were purchased from NatureWorks (USA) and SK Chemical (Korea), respectively. The multifunctional epoxy compatibilizer JONCRYL ADR4468 was supplied by BASF (Germany). PLA and PEICT pellets were dried at 80 °C for 12 h prior to the melt compounding process. The melt compounding was performed using a co-rotating twin-screw extruder (BA-19, Bautek, Korea) with a length/diameter (L/D) ratio of 40 and a screw diameter of 19 mm. The temperature profile of the individual heating zones from hopper to die was set to 190, 200, 210, 230, 230, 230, 220, and 210 °C, and the screw speed was set to 60 rpm. The components of the blends were dry mixed before the extrusion and fed through a single hopper. The blends were prepared with PLA/PEICT weight ratios denoted in Table 1. To prepare the ASTM standard specimens, the compounded blends were injection-molded (WIZ50E, LS Mtron, Korea) using a three-cavity mold. The melt and mold temperatures were 230 and 30 °C, respectively.

2.2. 2.2. Characterization

The wetting parameters of the blend components were calculated using contact angle measurements. The contact angle measurements were obtained using a SEO Phoenix contact angle analyzer equipped with a CDD camera (PHX-300, Surface Electro Optics, Korea). The contact angle between the substrate and the liquid was obtained using water and diiodomethane (75-11-6) (Sigma Aldrich, Korea) as the probe liquid. To determine the spreading coefficient at the processing temperature, a temperature coefficient of - 0.06 $mJm^{-2}K^{-1}$ was used [39].

Attenuated total reflection (ATR) Fourier transform infrared (FTIR) spectrometry (Nicolet IS30, Thermo Fisher Scientific, USA) measurements were used to determine the *in-situ* compatibilization of the blends. The FTIR spectra were measured at a resolution of 4 cm^{-1}, and 32 scans were averaged per experiment.

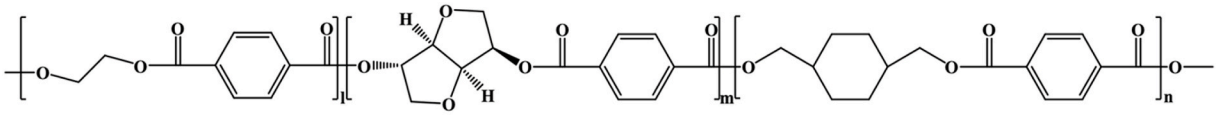

PEICT

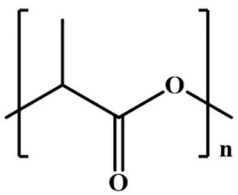

PLA

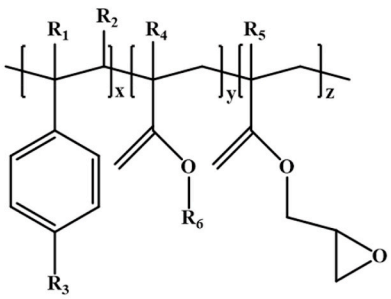

ADR

Scheme 1. Structures of poly(1,4-cyclohexane dimethylene isosorbide terephthalate) (PEICT); Chemical compositions determined by Yoon et al. l = 29.8 m = 22.7, and n = 47.2 [35], polylactide (PLA), and Joncryl ADR® (ADR).

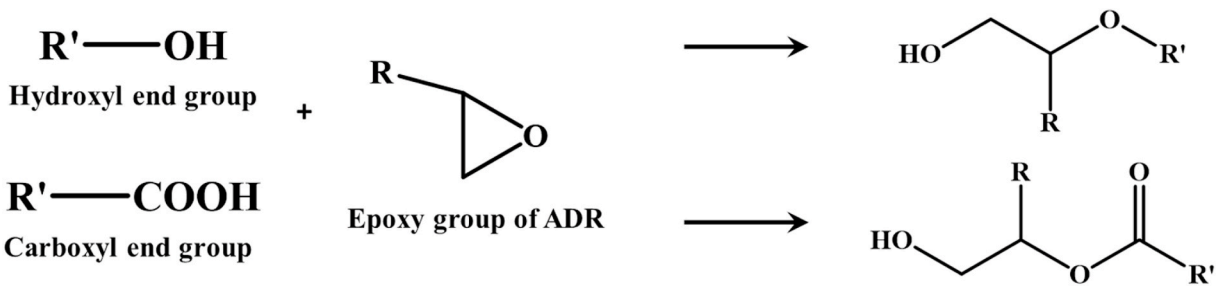

Scheme 2. Compatibilization reaction of ADR [49].

Table 1
Ratio of the PLA/PEICT blend components in wt%.

Designation	PLA	PEICT	ADR
PLA	100	0	0
PEICT	0	100	0
90/10	90	10	0
80/20	80	20	0
70/30	70	30	0
60/40	60	40	0
90/10A	89.25	10	0.75
80/20A	79.25	20	0.75
70/30A	69.25	30	0.75
60/40A	59.25	40	0.75

The rheological behaviors were analyzed using an advanced rheometric expansion system (ARES) (ARES, Rheometric Scientific, UK) fitted with two parallel plates. The frequency sweep tests were conducted at 230 °C with a frequency range of 0.1–500 Hz and a strain of 3%. The samples for the rheometric analysis were prepared by compression molding using 2-mm-thick disk molds having a diameter of 25 mm.

The morphologies of the cryo-fractured surfaces of the samples were observed using scanning electron microscopy (SEM) (JSM-6340F, JEOL, Japan). The injection-molded specimens were dipped in liquid nitrogen and quickly fractured to ensure that the morphology remained unchanged.

The tensile properties were investigated using a universal testing machine (Instron 4465, UK), following ASTM D638. The tensile measurements were performed using 10 KN loadcell at a speed of 95 mm/min. The speed of the tensile measurements was set to the size of the tensile specimen. Three-point bending tests according to ASTM D790 were performed using MCT-1150 (AND, Japan). Izod impact tests were performed according to ASTM D4812. At least five specimens were tested for each test, and average test values were taken. The thermal transitions of the blends were analyzed using differential scanning calorimetry (DSC) (DSC 2010, TA Instruments, USA). The samples were heated from 30 to 250 °C then quenched to 30 °C then reheated to 250 °C at a heating and cooling rate of 10 °C/min. Only the transitions from the second heating scan were considered to remove any previous thermal history. Thermogravimetric analysis (TGA) was performed using a Pyris 1 TGA (Perkin-Elmer, USA) over a temperature range of 30–700 °C and a heating rate of 10 °C/min. The thermal degradation was performed under a constant nitrogen flow of 100 mL/min to ensure a completely nonoxidative thermal degradation.

3. Results and discussion

3.1. Compatibilization of PLA/PEICT blends

Numerous studies have proposed theoretical models to predict the dispersion of the components in ternary blends. One of the frequently used models is the spreading coefficient proposed by Harkin [50]. Because the interfacial tension of the blend components thermodynamically determines the morphology of the ternary blend systems, the morphology can be predicted using the spreading coefficient. By rewriting Harkin's equation (eq. (1)), Hobbs et al. successfully predicted the morphology of immiscible ternary blend systems [51].

$$\lambda_{BC} = \gamma_{AC} - \gamma_{AB} - \gamma_{BC} \tag{1}$$

Here, λ_{BC} is the spreading coefficient of component B on component C inside matrix component A. In the case where λ_{BC} is positive and λ_{CB} is negative, C is encapsulated by B to form a core–shell structure. When both λ_{BC} and λ_{CB} are negative and λ_{AB} or λ_{AC} is negative, B is located at the interface of A and C. When both λ_{BC} and λ_{CB} are negative and λ_{AB} or λ_{AC} is positive, components B and C will form separate phases inside A [12]. The interfacial tensions (γ_{AB}) between two components A and B can be calculated using the Wu equation (harmonic mean equation, eq. (2)) [52] and Owens–Wendt equation (geometric mean equation, eq. (3)) [53].

$$\gamma_{AB} = \gamma_A + \gamma_B - 4\left(\frac{\gamma_A^d \gamma_B^d}{\gamma_A^d + \gamma_B^d} + \frac{\gamma_A^p \gamma_B^p}{\gamma_A^p + \gamma_B^p}\right) \tag{2}$$

$$\gamma_{AB} = \gamma_A + \gamma_B - 2\left(\sqrt{\gamma_A^d \gamma_B^d} + \sqrt{\gamma_A^p \gamma_B^p}\right) \tag{3}$$

Here, γ_A is the surface energy of component A and γ^d and γ^p denoted are the dispersive and polar contributions of the surface energies, respectively. The surface energies are calculated from the contact angle with the two-probe liquid water and diiodomethane [4]. The calculations were made using eqs. (4) and (5).

$$\gamma = \gamma^d + \gamma^p \tag{4}$$

$$\gamma_l(1 + \cos\theta) = \sqrt{2\left(\gamma_s^d \gamma_l^d\right)} + \sqrt{2\left(\gamma_s^p \gamma_l^p\right)} \tag{5}$$

The surface tensions of the blend components and the interfacial tensions between each pair of components are listed in Table 2. The blend components showed similar surface energy values where ADR had the highest surface energy of 48.99 mN/m and PEICT the lowest with 42.56 mN/m. Of the surface energy components, the dispersive force is dominant for all components in the blends. The higher dispersive contributions in the component polymers may result from the kink structure of polyesters. The sp2 hybridized orbitals from the aromatic rings in PEICT resulted in higher polar contributions than PLA. Among those of the blend components, the interfacial tension between PLA and ADR was the lowest (0.07 mN/m by harmonic mean and 0.03 mN/m by the geometric mean equation). PEICT and ADR had the second-lowest interfacial tension. On the basis of the lowest free energy principle for multi-component systems, the ADR would be located between PLA and PEICT. Furthermore, the spreading coefficient values are presented in Table 3 and are all negative values, indicating that ADR would spread at the interface of PLA and PEICT. These thermodynamic predictions made using the contact angle values imply that the ADR should be located at the interface of PLA and PEICT, allowing it to react with both PLA and PEICT.

The *in-situ* compatibilization of ADR occurs by the epoxy ring-

Table 2
Surface and interfacial energy of the blend components.

	Surface energy at 25 °C (mN/m)				Interfacial tension (γ_{ij}) at 230 °C (mN/m)	
Material	γ (25 °C)	γ (dispersive)	γ (polar)	Materials	Harmonic mean	Geometric mean
PLA	47.53	42.40	5.12	PLA/PEICT	0.91	0.46
PEICT	42.56	35.29	7.27	PLA/ADR	0.07	0.03
ADR	48.99	42.99	6.0	PEICT/ADR	0.94	0.47

Table 3
Spreading coefficient calculated using Harkin's equation.

	Spreading coefficient (mN/m)	
	Harmonic mean	Geometric mean
$\lambda_{PEICT/ADR}$	−1.79 (negative)	−0.90 (negative)
$\lambda_{ADR/PEICT}$	−0.09 (negative)	−0.05 (negative)
$\lambda_{PLA/ADR}$	−0.04 (negative)	−0.02 (negative)

opening reaction with the terminal carboxyl group or hydroxyl group of the polyesters. The FTIR spectra of pristine PLA and PEICT are shown in Fig. 1. The highlighted areas in Fig. 1 show the characteristic stretching frequencies of polyesters at 2950–2840 cm^{-1} for -CH, 1750–1720 cm-^{1} for C=O, and 1250–1020 cm^{-1} for C-O, as well as bending frequencies at 1480–1365 cm-1. Because of their structural differences, the characteristic absorption peaks appear at different locations for pristine PLA and PEICT. A sharp absorption peak for C=O stretching caused by ester groups is observed at 1746 cm^{-1} for PLA [39] and 1713 cm^{-1} for PEICT [35]. In addition, the C-O stretching peaks of the aliphatic ester in PLA appear at 1181 and 1080 cm^{-1}, whereas the aromatic ester peaks of PEICT appear at higher frequencies of 1253 and 1095 cm^{-1}.

The FTIR spectrum of the PLA/PEICT blend (60/40 ratio) shown in Fig. 1 contains absorption peaks at similar locations to those of pristine PLA and PEICT. The C=O stretching vibrations of the uncompatibilized blends show a split peak with similar intensities at 1752 and 1718 cm^{-1}. The presence of this split peak indicates the presence of both polymers in the blend. The split peak is also observed in the C-O twisting vibrations at 1182 and 1264 cm^{-1}. The ADR compatibilized blend also shows split peaks at the same location in the spectrum as that in the uncompatibilized blend. However, the intensity of the C=O stretching band at 1718 cm^{-1} corresponding to the C=O groups of PEICT is comparably lower than that of PLA at 1752 cm^{-1}. This phenomenon is also observed in the C-O twisting band at 1263 cm^{-1}. In addition, no additional peaks from

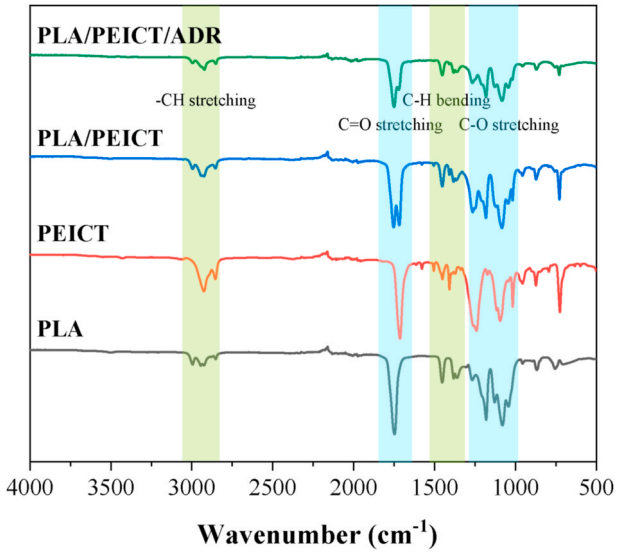

Fig. 1. FTIR spectra of PLA, PEICT, PLA/PEICT blend, and PLA/PEICT/ADR blend.

the added ADR were observed (i.e., the epoxy C-O stretching bands at 906 and 850 cm^{-1}), indicating the complete reaction of the ADR [39, 54, 55]. These results suggest the reaction between the epoxy groups of ADR and the carboxyl and hydroxyl chain ends of the two polyesters. The reacted polymers would, thus, form a copolymer with both PLA and PEICT chains, and these copolymers would act as surfactants to reduce the interfacial tension between PLA and PEICT.

The rheological properties of the samples observed at the processing temperature are shown in Fig. 2. In Fig. 2(a), the complex viscosities of pristine PLA and PEICT are compared with the complex viscosities of the prepared blends. PEICT showed somewhat Newtonian behavior with high viscosity at the processing temperature. In contrast, the processing temperature, which exceeds the conventional temperature for PLA, leads to noise-like viscosity distributions in the initial frequency range and comparably low-viscosity shear thinning behavior in the intermediate frequency range. The higher viscosity of the PEICT results from the stiffer structure induced by the aromatic ring and cyclic alkyls in the repeating unit. The PLA/PEICT blends showed similar curves to that of PLA, showing increasing viscosity and decreasing shear thinning behavior with increased PEICT content. However, with the addition of ADR, the PLA/PEICT blends showed a significantly higher zero shear viscosity and a prominent shear thinning behavior in the intermediate frequency region. The increased viscosity values and shear thinning behavior is a sign of interfacial interaction and entanglement caused by the *in-situ* compatibilization of ADR [39,41].

Plots of the storage (G′) and loss (G″) moduli against applied frequency for the prepared samples are shown in Fig. 2(b) and (c). The storage and loss moduli of viscoelastic materials under oscillatory stress is the energy stored elastically and dissipated during deformation. These values correspond to the elastic solid-like and viscous liquid-like behavior of the material. PEICT, a copolyester with rigid cyclic alkyl and aromatic rings and flexible alkyl spacers, exhibits excellent storage capabilities and high energy for deformation. The blending of PEICT with PLA increased both the storage and loss moduli with increasing PEICT content. Notably, at 10% PEICT content, the storage modulus in the lower frequency rate is lower than the pristine PLA. This is due to the low compatibility of the two blend components resulting in the plasticization of PLA with low PEICT content. Both the storage and loss modulus increase with the addition of ADR, and the moduli are even higher than those of PEICT, showing a synergetic increase. The synergetic increase in the moduli is caused by the lowering of the interfacial tension and chain entanglement, indicating the formation of copolymers by the *in-situ* reaction [28,41,46,56].

The SEM micrographs of cryo-fractured surfaces of the samples shown in Fig. 3 also support the formation of compatibilizing copolymers. The coalescence of the PEICT inside the PLA matrix in the PLA/PEICT blends resulted in the formation of spherical droplets, as shown in Fig. 3(a)–(d). The droplets are well-dispersed having even sizes, indicating that the processing method was adequate. Furthermore, the droplet size remained unchanged, even with the increased PEICT content and at the highest loading, indicating the compatibility between PEICT and PLA. After the *in-situ* compatibilization with ADR, PEICT droplets disappeared showing a single-phase (Fig. 3(a)'–3(d')). The appearance of a single phase is consistent with the spreading coefficient predicted using the contact angle measurements, where ADR is predicted to be located at the interface of the PEICT and PLA. Based on the FTIR results, the ADR reacted to form copolymers at the interface to

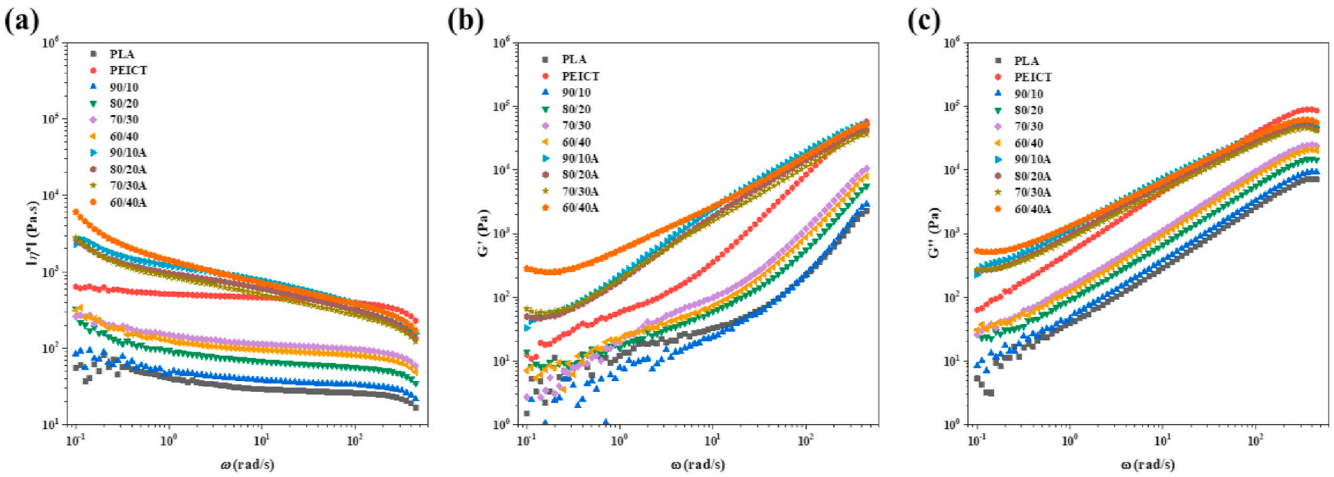

Fig. 2. (a) Complex viscosity, (b) storage modulus (G′), and (c) loss modulus (G″) of PLA/PEICT and PLA/PEICT/ADR blends.

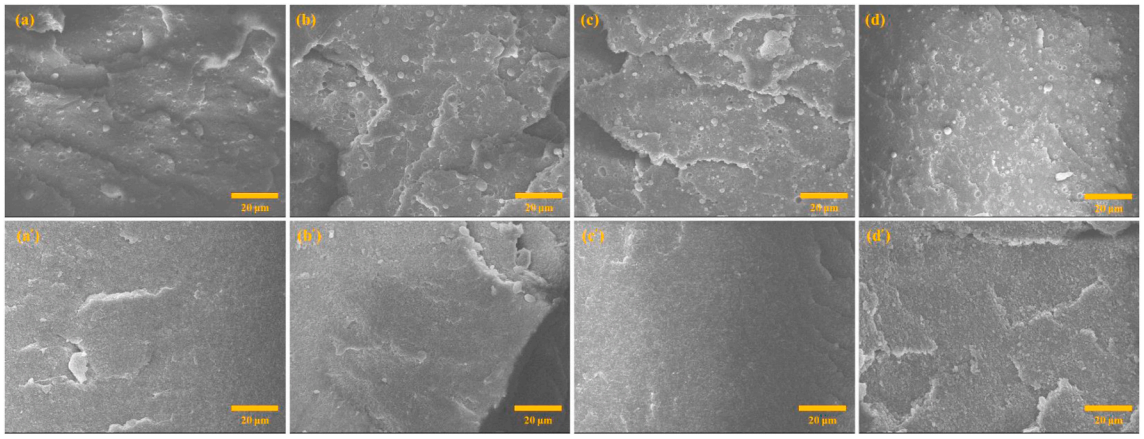

Fig. 3. SEM images of the cryo-fractured surfaces for (a) 90/10, (b) 80/20, (c) 70/30, (d) 60/40, (a') 90/10A, (b') 80/30A, (c') 70/30A, and (d') 60/40A. (×1000 magnification).

create a continuous phase.

3.2. Mechanical properties

The representative stress–strain curves, Young's moduli, and tensile strength of the PLA/PEICT blends are shown in Fig. 4(a)–(c), and the corresponding values are listed in Table 4. The Young's modulus and tensile strength of PLA are 1.66 GPa and 61.23 MPa, respectively, showing that PLA is a hard and brittle polymer. In contrast, PEICT is soft and ductile, having a Young's modulus and tensile strength of 0.93 GPa and 43.59 MPa. The addition of softer PEICT to PLA results in improved flexibility, as shown by the reduced modulus with increasing PEICT content. The PLA/PEICT blends showed a decrease in Young's modulus regardless of whether ADR was added, and as shown in Fig. 4(b), blends with the same PEICT content showed almost identical values. In contrast, the tensile strength of the PEICT blends showed opposite behaviors for blends with and without ADR. The blends without ADR showed increasing tensile strength with increasing PEICT content, which is interesting because virgin PEICT exhibits a comparably lower tensile strength than PLA. This phenomenon can be explained by the plasticizing effect of the incompatible PEICT in the rigid PLA. As shown in Fig. 4(a), at low contents, PEICT acts as a defect, leading to premature tensile break, whereas at higher contents, the plasticization effect of the PEICT droplets leads to higher tensile strengths. Although the tensile strength of the PLA/PEICT blends increases with increase in PEICT content, the PLA/PEICT blends exhibit lower strength than virgin PLA. However, after the addition of ADR, the tensile strength of 90/10A is higher than virgin PL, having a value of 65.29 MPa. The tensile strength of the blends with ADR decreases with increased PEICT content to 57.50 MPa for 60/40A. The decrease in the tensile strength is the result of unreacted PEICT domains residing in the blend because the amount of ADR was fixed at 0.75 wt%.

The flexural properties of the blends shown in Fig. 4(d) and (e) and listed in Table 4 are consistent with the tensile testing. The flexural modulus decreases for both PEICT/PLA blends and compatibilized blends, as did the tensile modulus; however, the compatibilized blends show lower flexural modulus and rate of decrease. The flexural strength of the PEICT/PLA blends shows a dramatic decrease with the increasing PEICT contains, whereas the compatibilized blends show a relatively gradual decrease. The low interfacial adhesion between the dispersed phases of PEICT and PLA resulted in the plasticization of PLA, leading to drastic failure during the three-point bend testing. On the other hand, the increased compatibility brought by the added ADR generated higher resistance to bending.

The impact strengths of the PLA/PEICT blends are presented in Fig. 4 (f). PLA is a brittle and hard polymer having an impact strength of 14.22 kJ/m^2, whereas PEICT does not break upon impact. The blending of PEICT with PLA toughened it, increasing the impact strength to 22.51 kJ/m^2 at 40% loading. As mentioned earlier, the low interfacial tension between PEICT and PLA led to the formation of small aggregates of PEICT that were well-dispersed in the PLA matrix. As depicted in Fig. 5, the small domains of PEICT in the PLA matrix acted as sites for impact

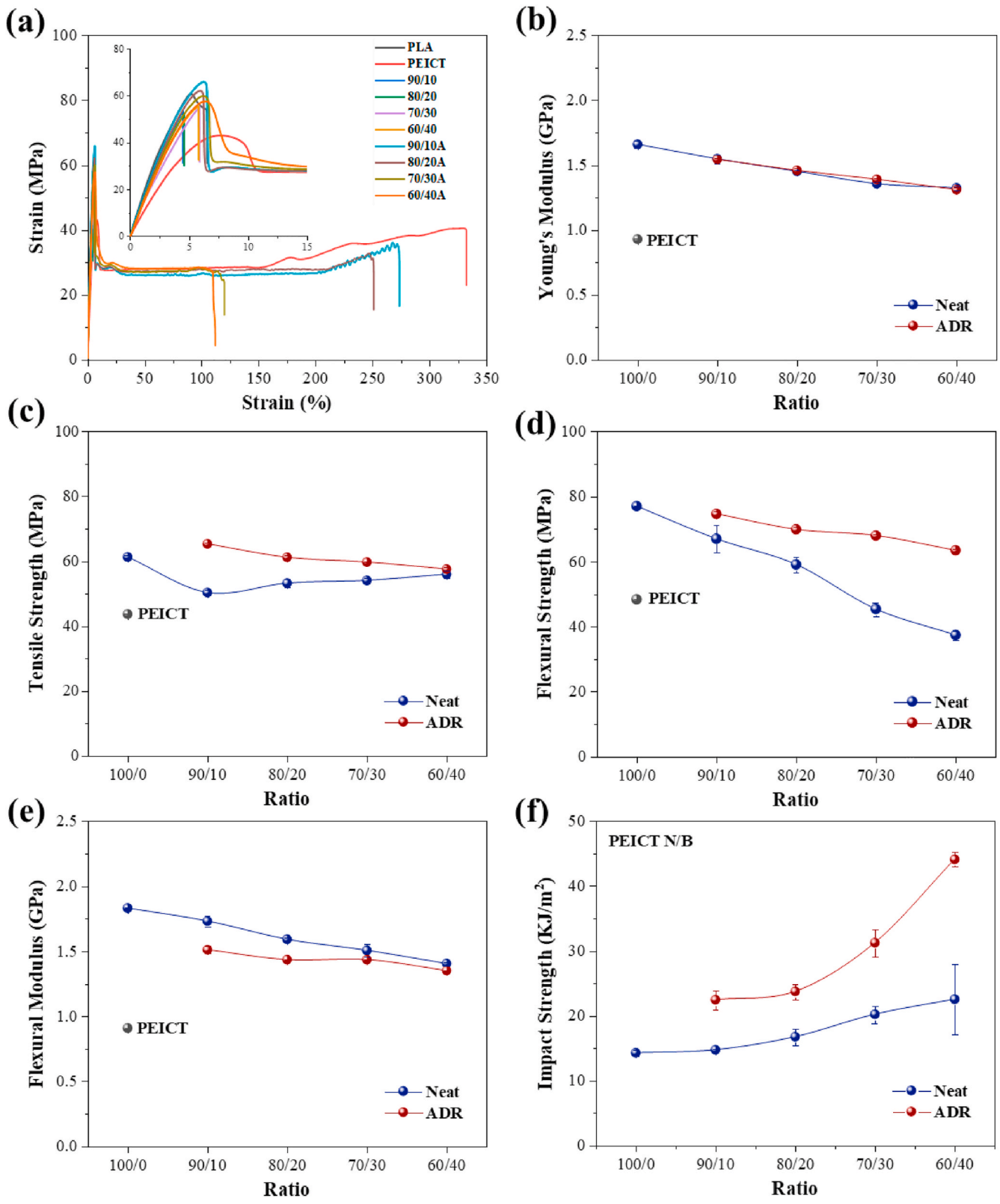

Fig. 4. Mechanical properties of PLA/PEICT blends, (a) stress–strain curves, (b) Young's modulus, (c) tensile strength, (d) flexural strength, (e) flexural modulus, and (f) impact strength.

energy consumption under high impact load, leading to higher impact strength. On the other hand, the blends with the ADR compatibilizer had an even higher increase in the impact strength with a value of 22 kJ/m^2 at just 10% PEICT, and a more drastic increase at 40% PEICT loading with an impact strength value of 44.11 kJ/m^2. The origin of this significant increase of impact properties is the result of the compatibilizing copolymer formed by the ADR reaction. These copolymers in the PLA/PEICT blends act as pathways for energy dissipation, transferring the

Table 4
Mechanical properties of PLA, PEICT, and PLA/PEICT.

	Young's modulus (GPa)	Tensile strength (MPa)	Flexural modulus (GPa)	Flexural strength (MPa)	Impact strength (kJ/m^2)
PLA	1.66 ± 0.03	61.23 ± 0.61	1.83 ± 0.00	77.03 ± 0.19	14.22 ± 0.54
PEICT	0.93 ± 0.01	43.59 ± 0.28	0.91 ± 0.01	48.27 ± 0.30	N/B
90/10	1.55 ± 0.03	50.26 ± 0.92	1.73 ± 0.04	66.98 ± 4.26	14.68 ± 0.25
80/20	1.45 ± 0.01	53.15 ± 1.22	1.59 ± 0.01	59.03 ± 2.39	16.71 ± 1.20
70/30	1.35 ± 0.01	53.98 ± 0.80	1.51 ± 0.05	45.30 ± 2.05	20.17 ± 1.36
60/40	1.32 ± 0.01	55.90 ± 1.24	1.40 ± 0.01	37.30 ± 1.44	22.51 ± 5.45
90/10A	1.54 ± 0.01	65.29 ± 0.53	1.51 ± 0.03	74.66 ± 0.87	22.43 ± 1.51
80/20A	1.46 ± 0.02	61.14 ± 0.60	1.43 ± 0.02	69.87 ± 0.63	23.71 ± 1.20
70/30A	1.39 ± 0.01	59.66 ± 0.27	1.43 ± 0.03	67.94 ± 0.34	31.24 ± 2.11
60/40A	1.31 ± 0.02	57.50 ± 0.71	1.35 ± 0.00	63.41 ± 0.57	44.11 ± 1.10

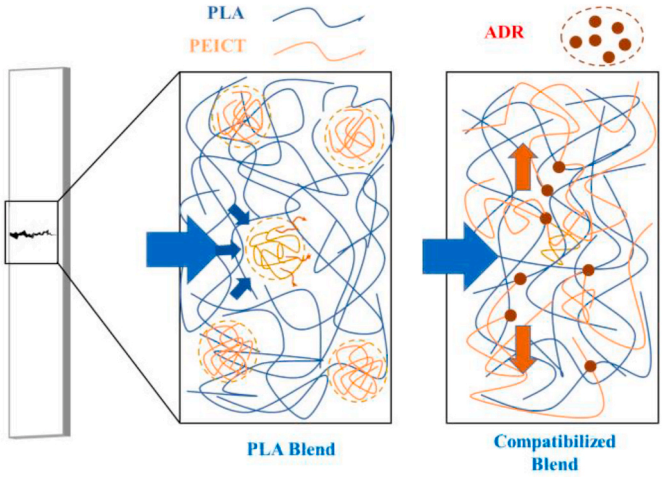

Fig. 5. Impact fracturing mechanism.

impact energy from PLA to the load-bearing PEICT [9,25,39].

3.3. Thermal properties

The DSC heating thermograms of PLA, PEICT and the PLA/PEICT blends are shown in Fig. 6, and their glass transition temperatures (Tg) are listed in Table 5. PLA and PEICT are immiscible amorphous polymers so the DSC thermograms show two baseline shifts representing Tg of each component. The Tg of neat PLA and neat PEICT were observed at 55.17 and 88.95 °C respectively, these values are consistent with other works [17,57,58]. When blended the Tg of both polymers occur at lower temperatures than its pristine state. This result might be due to the degradation of the polymer chains during the melt extrusion process. In the case of the PLA/PEICT blends the Tg of both PLA and PEICT increases with increasing PEICT composition. This increase in Tg is caused by the introduction of rigid structure in PEICT [59]. After the addition of ADR the Tg increase depending on PEICT composition is almost parallel to the uncompatibilized blends. However, both Tgs appear at a significantly higher temperatures when the blends are compatibilized. These results could be an indication of molecular weight increase for both components by the *in-situ* compatibilization reaction [39].

Fig. 7 shows the TGA and DTGA curves for PLA, PEICT, and PLA/

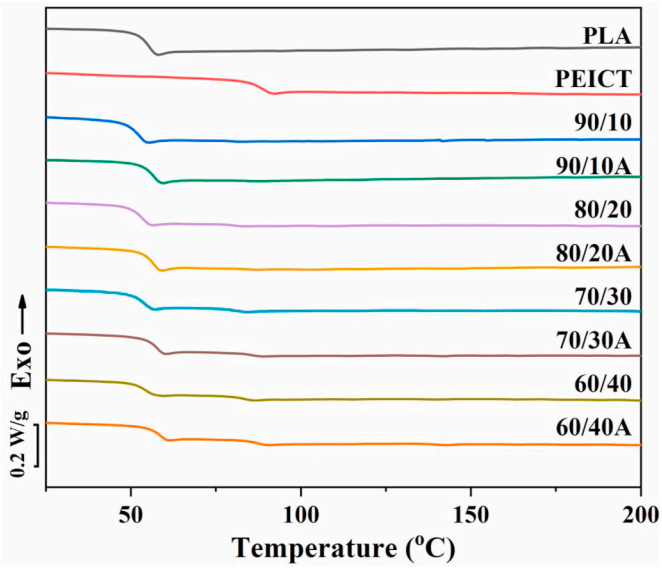

Fig. 6. DSC thermograms of pristine PLA, PEICT and PLA/PEICT blends.

Table 5
Glass transition temperatures of pristine PLA, PEICT, and PLA/PEICT blends.

	T_g (PLA) (°C)	T_g (PEICT) (°C)
PLA	55.17	–
PEICT	–	88.95
90/10	52.57	79.10
90/10A	56.81	85.39
80/20	53.66	80.49
80/20A	56.84	84.94
70/30	54.26	80.70
70/30A	57.91	85.87
60/40	54.45	83.86
60/40A	58.80	87.73

PEICT blends. All the PLA/PEICT blends show two-step thermal degradation, where the first step represents the degradation of PLA and the second step represents the degradation of PEICT. The second degradation peak of the blends occurred at a residual weight equivalent to the amount of PEICT added, indicating that the second degradation peak is the degradation of PEICT. As shown by the values in Table 6, the maximum degradation rate of PLA occurred at 453.3 °C and that of PEICT at 517.0 °C. The maximum degradation rate of all the PLA/PEICT blends corresponding to both PLA and PEICT was lower than the pristine polymer. These results could be due to the increased transesterification between PLA and PEICT [30,39,47]. Integral procedure decomposition temperature (IPDT) calculations (Table 6) yield similar values for both the pristine blends and the compatibilized blends.

4. Conclusions

The impact strength of PLA was improved using a biomass-based amorphous polymer PEICT and reactive compatibilizer ADR. The interfacial tension between each blend components calculated using contact angle, confirmed that the compatibilizer ADR would be located at the interface of PLA and PEICT. The FTIR spectroscopy and rheological analysis confirmed the formation of compatibilizing block copolymers by *in-situ* reaction. As the results of improved energy transfer between the polymers by compatibilization PLA/PEICT blend 60/40A reached Izod impact strength of 44.11 kJ/m^2. These results are comparable to high-impact polystyrene (HIPS) and acrylonitrile-butadiene-styrene (ABS) which are blends of polystyrene. Polystyrene is a commodity polymer also known for its brittleness and low impact strength

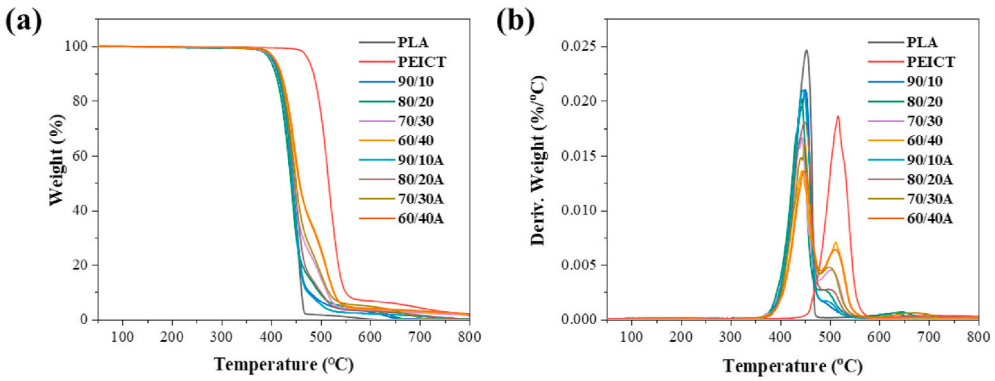

Fig. 7. TGA (a), and DTGA (b) curves for PLA/PEICT blends.

Table 6
Thermal degradation parameters of pristine PLA, PEICT, and PLA/PEICT blends.

	TGA in N_2 (°C)				T^e_{dm} (°C)	
	T_2[a]	T^b_{50}	T^c_{98}	IPDT[d]	Step 1	Step 2
PLA	390.8	444.2	468.0	460.0	453.3	
PEICT	463.8	516.3	769.8	556.0		517.0
90/10	386.7	444.0	612.8	467.3	450.5	489.2
80/20	383.2	440.2	629.0	466.8	443.0	499.8
70/30	386.0	445.0	720.8	488.0	444.0	503.7
60/40	392.0	456.5	771.3	506.5	444.2	512.3
90/10A	388.7	443.2	588.5	466.8	446.2	492.7
80/20/A	392.7	447.3	667.5	475.0	449.8	497.8
70/30A	394.0	450.7	668.2	483.2	450.0	499.8
60/40A	390.8	457.8	789.8	505.9	448.7	511.3

[a] Temperature at 2% weight loss.[b] Temperature at 50% weight los[s].[c] Temperature at 98% weight loss.[d] The integral procedure decomposition temperature, IPDT $= A\,K(T_f - T_i) + T_i$, where A is the area ratio of the total experimental curve, K is the coefficient parameter, T_i and T_f are the initial and final temperature [2].[e] Temperature at the maximum degradation rate.

and is blended to reach an unnotched impact strength of 27 kJ/m^2 for HIPS and 44 kJ/m^2 for ABS [60]. The results presented in this research shows a promising possibility of biobased PLA replacing commodity polymers and provides new applications to a newly commercialized copolyester.

Author statement

Chang Kyu Park performed conceptualization, investigation, visualization, and writing – original draft, reviewing and editing.

Dong Jin Jang performed investigation and visualization.

Joo Hyung Lee performed investigation and visualization.

Seong Hun Kim performed supervision*

Declaration of competing interest

The authors declare that they have no known competing financial interests or personal relationships that could have appeared to influence the work reported in this paper.

Acknowledgments

This research was supported by Basic Science Research Program through the National Research Foundation of Korea (NRF) funded by the Ministry of Education (NRF-2016R1A6A1A03013422 and NRF-2019R1F1A1062528).

References

[1] R.T. Mathers, How well can renewable resources mimic commodity monomers and polymers? Polym. Chem. 50 (2012) 1–15, https://doi.org/10.1002/pola.24939.
[2] E.J. Jeong, C.K. Park, S.H. Kim, Fabrication of microcellular polylactide/modified silica nanocomposite foams, J. Appl. Polym. Sci. 137 (2019) 48616–48625, https://doi.org/10.1002/app.48616.
[3] S.H. Park, S.G. Lee, S.H. Kim, Isothermal crystallization behavior and mechanical properties of polylactide/carbon nanotube nanocomposites, Compos. Part A-Appl. Sci. 46 (2013) 11–18, https://doi.org/10.1016/j.compositesa.2012.10.011.
[4] J.H. Bae, S.H. Kim, Alkylation of mixed micro- and nanocellulose to improve dispersion in polylactide, Polym. Int. 64 (2015) 821–827, https://doi.org/10.1002/pi.4858.
[5] R.E. Drumright, P.R. Gruber, D.E. Henton, Polylactic acid technology, Adv. Mater. 12 (2000) 1841–1846, https://doi.org/10.1002/1521-4095(200012)12:23<1841::AID-ADMA1841>3.0.CO;2-E.
[6] F. Carrasco, P. Pagès, J. Gámez-Pérez, O.O. Santana, M.L. Maspoch, Processing of poly (lactic acid): characterization of chemical structure, thermal stability and mechanical properties, Polym. Degrad. Stabil. 95 (2010) 116–125, https://doi.org/10.1016/j.polymdegradstab.2009.11.045.
[7] B. Wang, R. Ren, Z. Chen, Synthesis of cross-linked polylactide–poly (tetramethylene oxide) copolymers with enhanced toughness, Polym. Bull. 76 (2019) 1531–1541, https://doi.org/10.1007/s00289-018-2452-5.
[8] A.B. Kutikov, K.A. Reyer, J. Song, Shape-memory performance of thermoplastic amphiphilic triblock copolymer poly(d,l-lactic acid-co-ethylene glycol-co-d,l-lactic acid) (PELA)/hydroxyapatite composites, Macromol. Chem. Phys. 215 (2014) 2482–2490, https://doi.org/10.1002/macp.201400340.
[9] J.L. Atkinson, S. Vyazovkin, Thermal properties and degradation behavior of linear and branched poly(L-lactide)s and poly(L-lactide-co-glycolide)s, Macromol. Chem. Phys. 213 (2012) 924–936, https://doi.org/10.1002/macp.201100681;
[a] Y. Li, H. Shimizu, Toughening of polylactide by melt blending with a biodegradable poly(ether)urethane elastomer, Macromol. Biosci. 7 (2007) 921–928, https://doi.org/10.1002/mabi.200700027.
[10] K.S. Anderson, S.H. Lim, M.A. Hillmyer, Toughening of polylactide by melt blending with linear low-density polyethylene, J. Appl. Polym. Sci. 89 (2003) 3757–3768, https://doi.org/10.1002/app.12462.
[11] D. Yuan, J. Ding, W. Mou, Y. Wang, Y. Chen, Bio-based polylactide/epoxidized natural rubber thermoplastic vulcanizates with a co-continuous phase structure, Polym. Test. 64 (2017) 200–206, https://doi.org/10.1016/j.polymertesting.2017.10.011.
[12] F. Wu, M. Misra, A.K. Mohanty, Tailoring the toughness of sustainable polymer blends from biodegradable plastics via morphology transition observed by atomic force microscopy, Polym. Degrad. Stabil. 173 (2020) 109066–109076, https://doi.org/10.1016/j.polymdegradstab.2019.109066.
[13] M.A. Abdelwahab, A. Flynn, B.-S. Chiou, S. Imam, W. Orts, E. Chiellini, Thermal, mechanical and morphological characterization of plasticized PLA–PHB blends, Polym. Degrad. Stabil. 97 (2012) 1822–1828, https://doi.org/10.1016/j.polymdegradstab.2012.05.036.
[14] W. Meesorn, C. Calvino, J.C. Natterodt, J.O. Zoppe, C. Weder, Bio-inspired, self-toughening polymers enabled by plasticizer-releasing microcapsules, Adv. Mater. 31 (2019) 1807212–1807220, https://doi.org/10.1002/adma.201807212.
[15] G. Ozkoc, S. Kemaloglu, Morphology, biodegradability, mechanical, and thermal properties of nanocomposite films based on PLA and plasticized PLA, J. Appl. Polym. Sci. 114 (2009) 2481–2487, https://doi.org/10.1002/app.30772.
[16] I. Pillin, N. Montrelay, Y. Grohens, Thermo-mechanical characterization of plasticized PLA: is the miscibility the only significant factor? Polymer 47 (2006) 4676–4682, https://doi.org/10.1016/j.polymer.2006.04.013.
[17] H.N. Kim, C.K. Park, I.S. Kim, S.H. Kim, Compatibilization of immiscible blends of polypropylene and isosorbide containing copolyester with silica nanoparticles, Polym. Eng. Sci. 60 (2020) 1365–1376, https://doi.org/10.1002/pen.25387.
[18] J.H. Lee, S.H. Park, S.H. Kim, Surface alkylation of cellulose nanocrystals to enhance their compatibility with polylactide, Polymers 12 (2020) 178–195, https://doi.org/10.3390/polym12010178.

[19] J.H. Lee, S.H. Park, S.H. Kim, H. Ito, Replication and surface properties of micro injection molded PLA/MWCNT nanocomposites, Polym. Test. 83 (2020) 106321–106328, https://doi.org/10.1016/j.polymertesting.2019.106321.
[20] T. Talbamrung, C. Kasemsook, W. Sangtean, S. Wachirahuttapong, C. Thongpin, Effect of peroxide and organoclay on thermal and mechanical properties of PLA in PLA/NBR melted blend, Energy Procedia 89 (2016) 274–281. https://doi: 10.1016/j.egypro.2016.05.035.
[21] L. Jiang, J. Zhang, M.P. Wolcott, Comparison of polylactide/nano-sized calcium carbonate and polylactide/montmorillonite composites: reinforcing effects and toughening mechanisms, Polymer 48 (2007) 7632–7644, https://doi.org/10.1016/j.polymer.2007.11.001.
[22] L.G. Krauskopf, How about alternatives to phthalate plasticizers, J. Vinyl Addit. Technol. 9 (2004) 159–171, https://doi.org/10.1002/vnl.10079.
[23] A.P. Tüzüm Demir, S. Ulutan, Migration of phthalate and non-phthalate plasticizers out of plasticized PVC films into the air, J. Appl. Polym. Sci. 128 (2012) 1948–1961, https://doi.org/10.1002/app.38291.
[24] S.H. Myoung, S.S. Im, S.H. Kim, Non-isothermal crystallization behavior of PLA/acetylated cellulose nanocrystal/silica nanocomposites, Polym. Int. 65 (2016) 115–124, https://doi.org/10.1002/pi.5038.
[25] H. Chen, X. Yu, W. Zhou, S. Peng, X. Zhao, Highly toughened polylactide (PLA) by reactive blending with novel polycaprolactone-based polyurethane (PCLU) blends, Polym. Test. 70 (2018) 275–280, https://doi.org/10.1016/j.polymertesting.2018.07.023.
[26] M. Harada, K. Iida, K. Okamoto, H. Hayashi, K. Hirano, Reactive compatibilization of biodegradable poly(lactic acid)/poly(ε-caprolactone) blends with reactive processing agents, Polym. Eng. Sci. 48 (2008) 1359–1368, https://doi.org/10.1002/pen.21088.
[27] Z. Xu, Y. Zhang, Z. Wang, N. Sun, H. Li, Enhancement of electrical conductivity by changing phase morphology for composites consisting of polylactide and poly (ε-caprolactone) filled with acid-oxidized multiwalled carbon nanotubes, ACS Appl. Mater. Interfaces 3 (2011) 4858–4864, https://doi.org/10.1021/am201355j.
[28] D. Ji, Z. Liu, X. Lan, F. Wu, B. Xie, M. Yang, Morphology, rheology, crystallization behavior, and mechanical properties of poly(lactic acid)/poly(butylene succinate)/dicumyl peroxide reactive blends, J. Appl. Polym. Sci. 131 (2014) 39580–39587, https://doi.org/10.1002/app.39580.
[29] L. Xie, H. Xu, J.-B. Chen, Z.-J. Zhang, B.S. Hsiao, G.-J. Zhong, J. Chen, Z.-M. Li, From nanofibrillar to nanolaminar poly(butylene succinate): paving the way to robust barrier and mechanical properties for full-biodegradable poly(lactic acid) films, ACS Appl. Mater. Interfaces 7 (2015) 8023–8032, https://doi.org/10.1021/acsami.5b00294.
[30] H. Chen, M. Pyda, P. Cebe, Non-isothermal crystallization of PET/PLA blends, Thermochim. Acta 492 (2009) 61–66, https://doi.org/10.1016/j.tca.2009.04.023.
[31] C.L. Jun, Reactive blending of biodegradable polymers: PLA and starch, J. Polym. Environ. 8 (2000) 33–37, https://doi.org/10.1023/A:1010172112118.
[32] X. Yu, X. Wang, Z. Zhang, S. Peng, H. Chen, X. Zhao, High-performance fully bio-based poly(lactic acid)/polyamide11 (PLA/PA11) blends by reactive blending with multi-functionalized epoxy, Polym. Test. 78 (2019) 105980–105988, https://doi.org/10.1016/j.polymertesting.2019.105980.
[33] V. Gigante, I. Canesi, P. Cinelli, M.B. Coltelli, A. Lazzeri, Rubber toughening of polylactic acid (PLA) with poly(butylene adipate-co-terephthalate) (PBAT): mechanical properties, fracture mechanics and analysis of ductile-to-brittle behavior while varying temperature and test Speed, Eur. Polym. J. 115 (2019) 125–137, https://doi.org/10.1016/j.eurpolymj.2019.03.015.
[34] E. de C.D. Nunes, A.G. de Souza, D. dos S. Rosa, Effect of the Joncryl® ADR compatibilizing agent in blends of poly(butylene adipate-co-terephthalate)/poly (lactic acid), Macromol. Symp. 383 (2019) 1800035–1800040, https://doi.org/10.1002/masy.201800035.
[35] W.J. Yoon, S.Y. Hwang, J.M. Koo, Y.J. Lee, S.U. Lee, S.S. Im, Synthesis and characteristics of a biobased high-Tg terpolyester of isosorbide, ethylene glycol, and 1,4-cyclohexane dimethanol: effect of ethylene glycol as a chain linker on polymerization, Macromolecules 46 (2013) 7219–7231, https://doi.org/10.1021/ma4015092.
[36] S. Legrand, N. Jacquel, H. Amedro, R. Saint-Loup, J.-P. Pascault, A. Rousseau, F. Fenouillot, Synthesis and properties of poly(1,4-cyclohexanedimethylene-co-isosorbide terephthalate), a biobased copolyester with high performances, Eur. Polym. J. 115 (2019) 22–29, https://doi.org/10.1016/j.eurpolymj.2019. 03.018.
[37] R. Sablong, R. Duchateau, R. Koelewijn, C.E. Koning, G. de Wit, D. van Es, R. Koelewijn, J. van Haveren, Incorporation of isosorbide into poly(butylene terephthalate) via solid-state polymerization, Biomacromolecules 9 (2008) 3090–3097, https://doi.org/10.1021/bm800627d.
[38] D.-N. Phan, H. Lee, D. Choi, C.-Y. Kang, S.S. Im, I.S. Kim, Fabrication of two polyester nanofiber types containing the biobased monomer isosorbide: poly (ethylene glycol 1,4-cyclohexane dimethylene isosorbide terephthalate) and poly (1,4-cyclohexane dimethylene isosorbide terephthalate), Nanomaterials 8 (2018) 56–64, https://doi.org/10.3390/nano8020056.
[39] X. Wang, S. Peng, H. Chen, X. Yu, X. Zhao, Mechanical properties, rheological behaviors, and phase morphologies of high-toughness PLA/PBAT blends by in situ reactive compatibilization, Compos. B Eng. 173 (2019) 107028–107037, https://doi.org/10.1016/j.compositesb.2019.107028.
[40] Y. Chen, K. Chen, Y. Wang, C. Xu, Biobased heat-triggered shape-memory polymers based on polylactide/epoxidized natural rubber blend system fabricated via peroxide-induced dynamic vulcanization: Co-continuous phase structure, shape memory behavior, and interfacial compatibilization, Ind. Eng. Chem. Res. 54 (2015) 8723–8731, https://doi.org/10.1021/acs.iecr.5b02195.
[41] Y. Huang, C. Zhang, Y. Pan, W. Wang, L. Jiang, Y. Dan, Study on the effect of dicumyl peroxide on structure and properties of poly(lactic acid)/natural rubber blend, J. Polym. Environ. 21 (2012) 375–387, https://doi.org/10.1007/s10924-012-0544-0.
[42] M.-B. Coltelli, S. Bronco, C. Chinea, The effect of free radical reactions on structure and properties of poly(lactic acid) (PLA) based blends, Polym. Degrad. Stabil. 95 (2010) 332–341, https://doi.org/10.1016/j.polymdegradstab.2009.11.015.
[43] F. Yin, Q. Chen, J. Lin, Y. Deng, X. Mao, Effect of different peroxide initiators on the reaction extrusion of polypropylene-graft-cardanol and its compatibilization on PP/PC, J. Polym. Res. 21 (2014) 411–421, https://doi.org/10.1007/s10965-014-0411-x.
[44] B.-K. Chen, C.-H. Shen, S.-C. Chen, A.F. Chen, Ductile PLA modified with methacryloyloxyalkyl isocyanate improves mechanical properties, Polymer 51 (2010) 4667–4672, https://doi.org/10.1016/j.polymer.2010.08.028.
[45] Y. Baimark, P. Srihanam, Influence of chain extender on thermal properties and melt flow index of stereocomplex PLA, Polym. Test. 45 (2015) 52–57, https://doi.org/10.1016/j.polymertesting.2015.04.017.
[46] F. Walha, K. Lamnawar, A. Maazouz, M. Jaziri, Rheological, morphological and mechanical studies of sustainably sourced polymer blends based on poly(lactic acid) and polyamide 11, Polymers 8 (2016) 61–83, https://doi.org/10.3390/polym8030061.
[47] X. Li, X. Ai, H. Pan, J. Yang, G. Gao, H. Zhang, H. Yang, L. Dong, The morphological, mechanical, rheological, and thermal properties of PLA/PBAT blown films with chain extender, Polym. Adv. Technol. 29 (2018) 1706–1717, https://doi.org/10.1002/pat.4274.
[48] X. Li, X. Yan, J. Yang, H. Pan, G. Gao, H. Zhang, L. Dong, Improvement of compatibility and mechanical properties of the poly(lactic acid)/poly(butylene adipate-co-terephthalate) blends and films by reactive extrusion with chain extender, Polym. Eng. Sci. 58 (2018) 1868–1878, https://doi.org/10.1002/pen.24795.
[49] D. Nakayama, F. Wu, A.K. Mohanty, S. Hirai, M. Misra, Biodegradable composites developed from PBAT/PLA binary blends and silk powder: compatibilization and performance evaluation, ACS Omega 3 (2018) 12412–12421. https://10.1021/acsomega.8b00823.
[50] W.D. Harkins, A. Feldman, Films. the spreading of liquids and the spreading coefficient, J. Am. Chem. Soc. 44 (1922) 2665–2685, https://doi.org/10.1021/ja01433a001.
[51] S.Y. Hobbs, M.E.J. Dekkers, V.H. Watkins, Effect of interfacial forces on polymer blend morphologies, Polymer 29 (1988) 1598–1602, https://doi.org/10.1016/0032-3861(88)90269-8.
[52] S. Wu, Polymer Interfacial and Adhesion, Marcel Dekker Inc., New York, 1982.
[53] D.K. Owens, R.C. Wendt, Estimation of the surface free energy of polymers, J. Appl. Polym. Sci. 13 (1969) 1741–1747, https://doi.org/10.1002/app.1969.070130815.
[54] R. Al-Itry, K. Lamnawar, A. Maazouz, Improvement of thermal stability, rheological and mechanical properties of PLA, PBAT and their blends by reactive extrusion with functionalized epoxy, Polym. Degrad. Stabil. 97 (2012) 1898–1914, https://doi.org/10.1016/j.polymdegradstab.2012.06.028.
[55] A.L. Perrone de L. Freitas, L.R.T. Filho, P.S. Calvão, A.M. Catelli de Souza, Effect of montmorillonite and chain extender on rheological, morphological and biodegradation behavior of PLA/PBAT blends, Polym. Test. 62 (2017) 189–195, https://doi.org/10.1016/j.polymertesting.2017.06.030.
[56] L. Gu, E.E. Nessim, C.W. Macosko, Reactive compatibilization of poly(lactic acid)/polystyrene blends and its application to the preparation of hierarchically porous poly(lactic acid), Polymer 134 (2018) 104–116, https://doi.org/10.1016/j.polymer.2017.11.054.
[57] X. You, M.R. Snowdon, M. Misra, A.K. Mohanty, Biobased poly(ethylene terephthalate)/poly(lactic acid) blends tailored with epoxide compatibilizers, ACS Omega 3 (2018) 11759–11769. https://10.1021/acsomega.8b01353.
[58] A.R. McLauchlin, O.R. Ghita, Studies on the thermal and mechanical behavior of PLA-PET blends, J. Appl. Polym. Sci. 133 (2016) 44147–44158, https://doi.org/10.1002/app.44147.
[59] V. Thitha, R. Lehman, T. Nosker, Morphological effects on glass transition behavior in selected immiscible blends of amorphous and semicrystalline polymers, Polymer 47 (2006) 5392–5401, https://doi.org/10.1016/j.polymer.2006.05.014.
[60] L.B. Brennan, D.H. Isaac, J.C. Arnold, Recycling of acrylonitrile–butadiene–styrene and high-impact polystyrene from waste computer equipment, J. Appl. Poym. Sci. 86 (2002) 572–578, https://doi.org/10.1002/app.10833.